

Supplementary Information

## **Hotspots and Hot Moments of Metal Mobilization: Dynamic Connectivity in Legacy Mine Waters**

Anita Alexandra Sanchez<sup>1,2\*</sup>, Maximilian P. Lau<sup>1,2</sup>, Sean Adam<sup>1,3</sup>, Sabrina Hedrich<sup>1,4</sup>, & Conrad Jackisch<sup>1,3</sup>

<sup>1</sup>Interdisciplinary Environmental Research Centre, Technische Universität Bergakademie Freiberg, Freiberg, 09599, Germany

<sup>2</sup>Institute of Mineralogy, Technische Universität Bergakademie Freiberg, Freiberg, 09599, Germany

<sup>3</sup>Institute of Drilling Technology and Fluid Mining, Technische Universität Bergakademie Freiberg, Freiberg, 09599, Germany

<sup>4</sup>Institute of Biosciences, Technische Universität Bergakademie Freiberg, Freiberg, 09599, Germany

*Correspondence to:* Anita Alexandra Sanchez (Anita.Sanchez@mineral.tu-freiberg.de)

## Contents

|  |          |
|--|----------|
| <b>Section S1.</b> Supplementary Information on methodology.....                             | page S3  |
| • <i>Hydrological data collection and analysis</i>   |          |
| • <i>Spectral processing and cubist model calibration</i>                                    |          |
| <b>Section S2.</b> Supplementary Information on characteristics of sampled locations.....    | page S4  |
| • <i>Physicochemical parameters of four sites in Reiche Zeche Mine</i>                       |          |
| <b>Section S3.</b> Supplementary Information on spatial and temporal trends.....             | page S5  |
| • <i>Dynamics of four sites compared to other sampling sites</i>                             |          |
| • <i>Metal(loid) loads for each flow phase across two years</i>                              |          |
| <b>Section S4.</b> Supplementary Information on C-Q relationships and spectrolyzer data..... | page S8  |
| • <i>C-Q slopes across two years</i>   |          |
| • <i>C-Q hysteresis index values for each flow phase across two years</i>                    |          |
| <b>Section S5.</b> Supplementary Information on cubist modeling results.....                 | page S10 |
| • <i>Cubist modeling</i>   |          |

## Section S1. Supplementary Information on methodology

**Hydrological data collection and analysis.** Water level loggers (Levellogger 5, Solinst Canada Ltd.) were installed at sites 1, 2, 3A, and 3B, where the water level and flow could be continuously monitored and quantified. The water level loggers at levels 1 and 2 recorded measurements from March 2022 to approximately January 2024 and the loggers at levels 3A and 3B recorded measurements from February 2022 to March 2024. The “Levellogger Software 4.6.2” was used to retrieve the recorded data. For precise measurement of water levels and flow at the outflow points of sites 1 and 2, plastic weirs were constructed and installed. Conversely, sites 3A and 3B were equipped with small spillways instead of weirs. The measurements obtained were critical for establishing the relationships between water levels and discharge rates. From Henderson (1996), the formula for triangular measuring weirs was used:

$$Q = \frac{8}{15} * C_d * \sqrt{2 * g} * \tan\left(\frac{\alpha}{2}\right) * h^{\frac{5}{2}} \quad (1)$$

where  $Q$  is the flow rate (in  $\text{m}^3/\text{s}$ ],  $C_d$  is the discharge coefficient,  $g$  is the gravitational constant ( $9.81 \text{ m/s}^2$ ),  $\alpha$  is the angle of the lower weir edge ( $^\circ$ ) and  $h$  is the water level above the outlet (m). The water level-discharge relationship was applied at sites 1, 2, 3A, and 3B. A non-linear regression was used to transfer the data and using the Savitzky-Golay filter, the flows were correctly processed. Using the flow rate data, we identified different flow phases by observing flow rate patterns for each site and assigned each flow phase to a certain date range.

The stable isotopic composition of  $\delta^2\text{H}$  and  $\delta^{18}\text{O}$  were measured using cavity ring-down spectroscopy. Reference materials were measured as standards at the beginning of the measurements. All mine water samples collected at the four sites were measured eight times. The first three measurements were discarded, and the remaining measurements were weighted according to their position and using a hyperbolic fit. The hyperbolic values of the measurements were corrected using the standard values. Manual calibrations were continuously performed. From the  $\delta^2\text{H}$  and  $\delta^{18}\text{O}$  isotope data of surface precipitation, the LMWL was created. The LMWL indicates the regional meteoric influences on isotopic fractionation and is compared with the isotopic composition of the global precipitation using the GMWL formula (Craig, 1961):

$$\delta^2\text{H} = 8 * \delta^{18}\text{O} + 10 \quad (2)$$

The LMWL served as a reference for mine water samples to determine the origin of the mine water and variability of the samples collected. Several samples may be more strongly influenced by precipitation, or their isotopic composition may be more similar to “old” water or “young” water entering the mine.

***Spectral processing and cubist model calibration.*** Chemometric models were calibrated from UV-Vis scans (i.e., measurements from the online UV-Vis spectrometer device, referred to as spectrolyzer here on) and corresponding analytical data (i.e., measurements from the Autosampler) to predict trace element concentrations.

UV-Vis spectra were recorded from 200 to 720 nm at a resolution of 0.5 nm. Raw spectra were cleaned by removing implausible scans (absorbance < 0 or absorbance > 4.5). Spectra were processed using the `prospectr` package Stevens and Ramirez-Lopez (2022). First, spectra were smoothed using a Savitzky Golay filter with a polynomial degree of 3 and a window size of 11 to remove noise. Then, a Standard Normal Variate (SNV) correction was applied. Both raw, smoothed and smoothed + snv-corrected spectra were used for model calibration.

Chemometric models were calibrated using the Cubist package Kuhn and Quinlan (2023) in the caret framework Kuhn (2008) for the following dissolved metal(loid)s: Mn, Ni, As, Cd, Pb, Fe, Al, Cu, and Zn. Models were calibrated both for untransformed and log1p-transformed variables, and using the three differently processed spectral sets (raw, smoothed, smoothed+snv). Cubist models were tuned for 1, 2, 5, 10, 20, and 50 committees and 0-9 neighbors using a 10-fold cross-validation. 75 % of the dataset was used for calibration and 25 % was held back for testing. The dataset was split using random, percentile-binned sampling. Model accuracy was evaluated using the test set, using a modified version of the `evaluate_model()` function found in the `simplerspec` package Baumann (2020) to calculate RMSE, R2, RPD, and Lin's concordance correlation coefficient among other valuation statistics. An example for the predictions for the test set can be seen in section S4.

## **Section S2. Supplementary Information on characteristics of sampled locations**

***Reiche Zeche mine.*** Selected physicochemical parameters of sites sampled in Reiche Zeche collected for the entire two-year sampling period in all three levels and the central drainage adit were obtained. These parameters included: pH, Electrical Conductivity (EC), Dissolved Organic Carbon (DOC), Dissolved Inorganic Carbon (DIC), and dissolved metal(loid) concentrations. All analyses were performed in the laboratory. The number of samples (n) obtained for each site were averaged ( $\pm$  standard error) and used as a comparison to highlight the quantitative differences between the four sites and are provided in **Supplementary Table S1**.

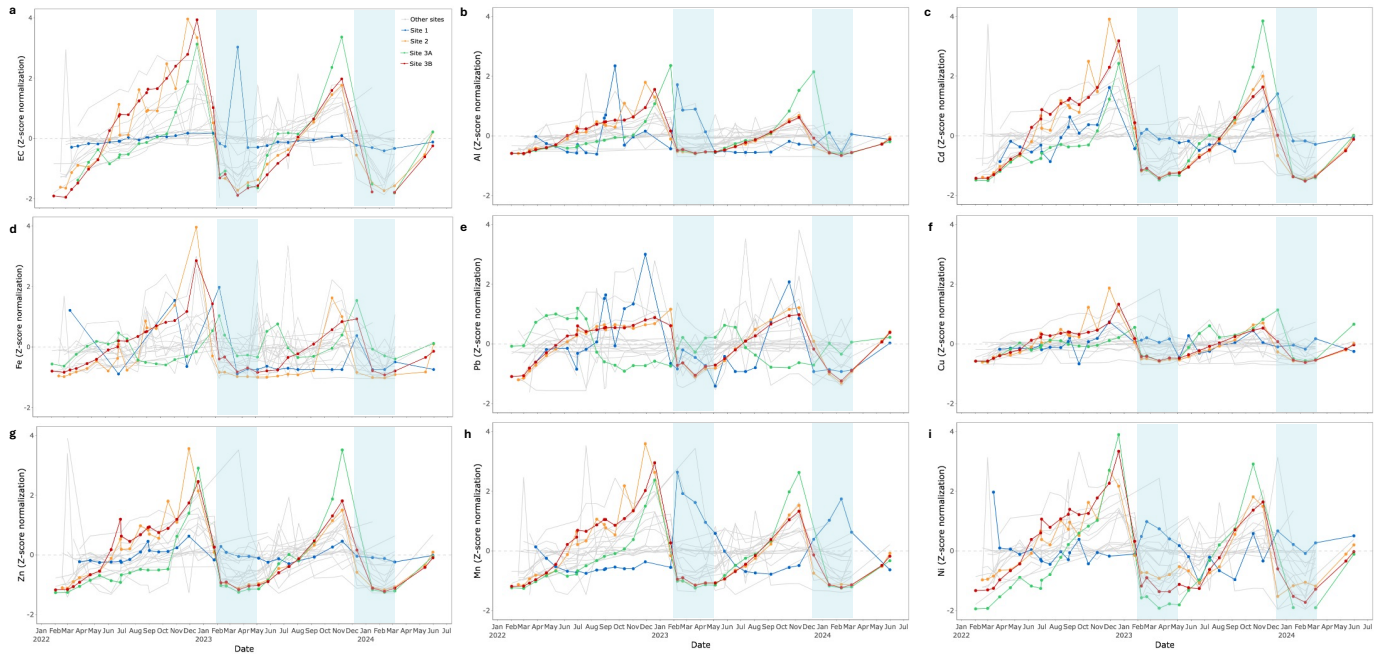
**Supplementary Table S1.** Average values and standard errors (SE) of physicochemical parameters of water sampling sites from several locations of Schwarzer Hirsch Stehender, Reiche Zeche. Standard error was calculated as  $SE = SD/\sqrt{n}$ , where SD is the standard deviation and n is the number of samples per site. NA refers to values being below the limit of detection.

|                       | Site 1 |       |       |        |    | Site 2 |       |       |       |    | Site 3A |       |       |       |    | Site 3B |       |       |       |    |
|-----------------------|--------|-------|-------|--------|----|--------|-------|-------|-------|----|---------|-------|-------|-------|----|---------|-------|-------|-------|----|
| Parameters            | Mean   | Min   | Max   | SE     | n  | Mean   | Min   | Max   | SE    | n  | Mean    | Min   | Max   | SE    | n  | Mean    | Min   | Max   | SE    | n  |
| pH                    | 5.5    | 3.7   | 6.4   | 0.09   | 32 | 3.5    | 3.0   | 4.1   | 0.05  | 37 | 3.1     | 2.9   | 3.7   | 0.03  | 34 | 3.3     | 2.9   | 3.9   | 0.05  | 37 |
| EC( $\mu$ S/cm)       | 320    | 290   | 549   | 7.65   | 32 | 552    | 328   | 1066  | 31.1  | 37 | 1097    | 545   | 2350  | 82.1  | 34 | 725     | 366   | 1396  | 44.6  | 37 |
| Q (mL/s)              | 280    | 53.6  | 893   | 44.9   | 25 | 166    | 5.49  | 670   | 36.3  | 28 | 285     | 125   | 596   | 21.1  | 33 | 285     | 116   | 720   | 27.8  | 33 |
| $\delta^2\text{H}$    | -60.0  | -66.9 | -49.7 | 0.50   | 32 | -60.5  | -67.0 | -43.7 | 0.58  | 34 | -61.6   | -66.9 | -59.9 | 0.23  | 33 | -61.0   | -65.1 | -57.4 | 0.23  | 35 |
| $\delta^{18}\text{O}$ | -8.90  | -10.1 | -5.32 | 0.14   | 32 | -8.95  | -10.3 | -3.13 | 0.19  | 34 | -9.22   | -10.4 | -8.92 | 0.05  | 33 | -9.09   | -9.73 | -8.56 | 0.05  | 35 |
| DOC(mg/L)             | 1.2    | 0.73  | 1.9   | 0.05   | 32 | 1.3    | 0.86  | 2.3   | 0.06  | 37 | 1.8     | 0.66  | 8.1   | 0.24  | 34 | 1.5     | 0.85  | 7.2   | 0.17  | 37 |
| DIC(mg/L)             | 0.71   | 0.00  | 2.0   | 0.06   | 32 | 0.33   | 0.00  | 0.90  | 0.03  | 37 | 0.40    | 0.00  | 1.1   | 0.04  | 34 | 0.30    | 0.00  | 0.96  | 0.03  | 37 |
| Fe(mg/L)              | 0.02   | 0.003 | 0.26  | 0.008  | 32 | 3.7    | 0.08  | 23    | 0.97  | 37 | 3.3     | 0.27  | 8.1   | 0.27  | 34 | 2.4     | 0.29  | 9.2   | 0.32  | 37 |
| Zn(mg/L)              | 1.6    | 1.3   | 2.3   | 0.05   | 32 | 14     | 2.7   | 49    | 1.8   | 37 | 106     | 14    | 477   | 21    | 34 | 28      | 4.3   | 75    | 3.2   | 37 |
| Pb(mg/L)              | 0.06   | 0.009 | 0.16  | 0.006  | 32 | 1.0    | 0.23  | 1.8   | 0.08  | 37 | 0.90    | 0.42  | 1.6   | 0.06  | 34 | 1.2     | 0.3   | 2.0   | 0.08  | 37 |
| Cd(mg/L)              | 0.013  | 0.007 | 0.025 | 0.001  | 32 | 0.13   | 0.025 | 0.42  | 0.02  | 37 | 0.83    | 0.24  | 3.3   | 0.14  | 34 | 0.27    | 0.030 | 0.74  | 0.03  | 37 |
| Cu(mg/L)              | 0.018  | 0.002 | 0.037 | 0.001  | 32 | 0.35   | 0.063 | 1.26  | 0.05  | 37 | 1.6     | 0.35  | 4.0   | 0.16  | 34 | 0.70    | 0.12  | 2.0   | 0.07  | 37 |
| Al(mg/L)              | 0.047  | 0.006 | 0.21  | 0.009  | 32 | 2.6    | 0.39  | 9.9   | 0.39  | 37 | 16      | 2.4   | 73    | 3.1   | 34 | 4.9     | 0.29  | 17    | 0.64  | 37 |
| Mn(mg/L)              | 0.067  | 0.032 | 0.19  | 0.008  | 32 | 1.1    | 0.25  | 3.9   | 0.15  | 37 | 7.3     | 1.2   | 32    | 1.3   | 34 | 2.2     | 0.40  | 6.6   | 0.26  | 37 |
| Ni(mg/L)              | 0.011  | 0.007 | 0.015 | 0.0003 | 32 | 0.022  | 0.01  | 0.04  | 0.001 | 37 | 0.070   | 0.019 | 0.24  | 0.009 | 34 | 0.030   | 0.011 | 0.066 | 0.002 | 37 |
| As(mg/L)              | NA     | NA    | NA    | NA     | 32 | 0.11   | 0.10  | 0.23  | 0.005 | 37 | NA      | NA    | NA    | 0.00  | 34 | NA      | NA    | NA    | NA    | 37 |

### Section S3. Supplementary Information on spatial and temporal trends

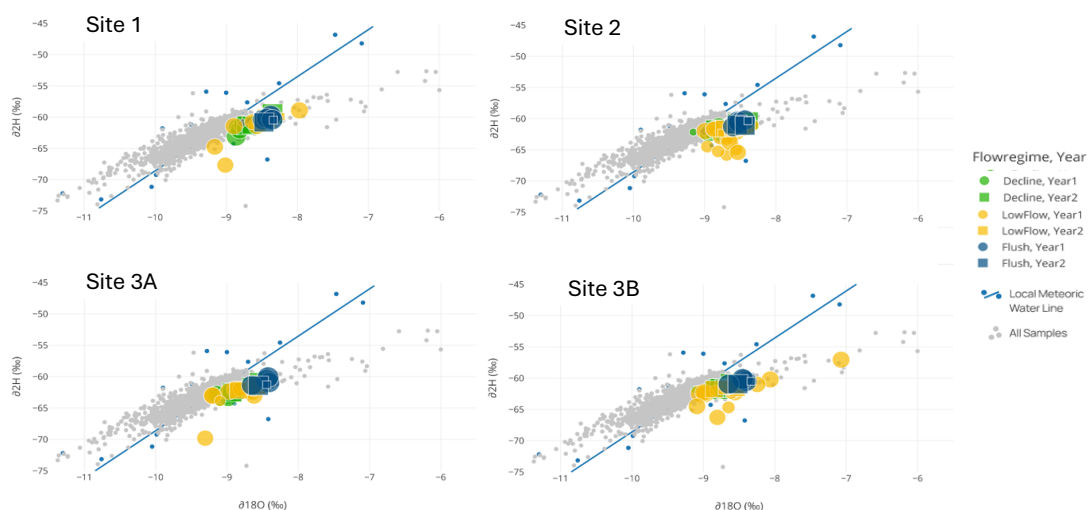
**Dynamics of four sites compared to other sampling sites.** The temporal trends of dissolved metals at sites 1, 2, 3A, and 3B were compared to other sites among the three levels within Reiche Zeche from February 2<sup>nd</sup>, 2022 to May 31<sup>st</sup>, 2024 (**Supplementary Figure S1 a-i**). All four sites exhibit distinct episodic surges in dissolved Fe, Zn, Al, Cd, Pb, Cu, Mn, and Ni, with concentrations rising sharply and then returning to baseline levels. Sites 3A and 3B tend to have the largest accumulation of metal concentrations right before the occurrence of each flush phase, which then causes a great dilution of the present metals. These high-release events suggest that metal(loid) mobilization originates from material in contact with the deeper water layers rather than the surface outflow. The timing of these events appears seasonal, likely influenced by hydrological or biogeochemical triggers such as stratification development during low flow, breakdown during high flow or shifts in associated redox conditions. In contrast to the trends observed for the other metals, dissolved Pb concentrations remained relatively stable across all sites (except site 1), suggesting that Pb may be present in generally lower quantities at

the deeper sites or that it is less susceptible to episodic mobilization under varying hydrological conditions. In addition, metal concentrations at the other sites among the RZ levels remain low and relatively stable over time.



**Supplementary Figure S1:** Spatial and temporal dynamics in (a) electrical conductivity, dissolved (b) Al, (c) Cd, (d) Fe, (e) Pb, (f) Cu, (g) Zn, (h) Mn, and (i) Ni concentrations across the mine system. Values are z-scaled, i.e. dissolved Al concentrations are visualized in standard deviations away from the site mean. Individual sites are connected by black lines and colored lines are monitored flow sites for sites 1, 2, 3A, and 3B. The blue panel highlights the year 1 and 2 flush period.

The spatial synchrony in geochemical responses across mine levels suggest a system-wide process of transient hydrological connectivity further shown through isotopic analyses of  $\delta^2\text{H}$  and  $\delta^{18}\text{O}$  (**Supplementary Figure S2**). During low and declining flow phases, samples collected at all four sites exhibited stable isotopic signatures clustering near the Local Meteoric Water Line (LMWL), indicative of mixing with older, stored water. In contrast, during flush phases, isotopic compositions deviated from the background, trending toward more younger signatures. This shift suggests rapid mobilization of recent meteoric inputs along reactivated pathways (Spangenberg et al., 2007; Swenson et al., 2024). The similarity in isotopic patterns across years and sites reinforces the presence of a recurrent threshold-driven connectivity regime, wherein hydrological re-connectivity causes a pulse-like release of fresher water.



**Supplementary Figure S2:** Isotope signatures of the water samples collected at sites (a) 1, (b) 2, (c) 3A, and (d) 3B are shown. The blue line presents the local meteoric water line. In the background, all samples from the project until March 2024 are shown in grey. Green markers present the declining flow phase, yellow markers display the low flow phase, and blue markers present the flush phase with marker shapes differentiating between the two years (circle - year 1; square - year 2).

***Metal(loid) loads for each flow phase across two years.*** **Supplementary Table S2** summarizes the quantity of dissolved metal(loid) loads (kg/day) across declining, low, and flush flow phases for sites 1, 2, 3A, and 3B during years 1 and 2. A clear pattern emerges where sites 2, 3A, and 3B consistently exhibited the highest total metal loads during low flow periods, especially for Zn, Al, Fe, and Mn, indicating substantial mobilization from persistent, slowly accessed subsurface sources. In contrast, site 1 showed peak loads during the flush phase, consistent with shorter residence times and faster hydrological turnover. Zn dominated the load profile across all deeper sites, with year 1 values during low flow reaching over 30 kg/day at site 3A, underscoring its major role in overall contaminant flux. Notably, Cd loads remained relatively low across all sites, but their persistence across phases, particularly at sites 2 and 3B, supports the interpretation of diffuse and conservative transport behavior. Meanwhile, Pb, Cu, and Ni showed more variability between sites and years, with site 3A standing out as a potential hotspot in both years. Interannual differences were also evident. While site 2's total loads were similar between years, sites 3A and 3B displayed significantly higher values in year 1 for most metal(loid)s, particularly Zn and Al. These differences likely reflect greater system connectivity following drier periods at these deeper sites.

**Supplementary Table S2.** Quantity of dissolved metal(loid) loads for year 1 and 2 of declining, low flow, and flush phases for each site. NA refers to metal(loid) loads not quantified due to insufficient discharge data or concentration values below the detection limit.

| Metal(loid)<br>load (kg/d) | Year | Site 1            |             |       | Site 2            |             |        | Site 3A           |             |       | Site 3B           |             |       |
|----------------------------|------|-------------------|-------------|-------|-------------------|-------------|--------|-------------------|-------------|-------|-------------------|-------------|-------|
|                            |      | Declining<br>Flow | Low<br>Flow | Flush | Declining<br>Flow | Low<br>Flow | Flush  | Declining<br>Flow | Low<br>Flow | Flush | Declining<br>Flow | Low<br>Flow | Flush |
| Fe                         | 1    | 0.0003            | 0.003       | 0.005 | 0.050             | 0.295       | 0.099  | 0.368             | 0.790       | 0.649 | 0.106             | 0.751       | 0.213 |
| Zn                         | 1    | 0.125             | 0.200       | 0.381 | 0.293             | 1.150       | 0.856  | 4.703             | 30.791      | 4.256 | 1.273             | 8.233       | 1.633 |
| Cd                         | 1    | 0.0009            | 0.002       | 0.003 | 0.003             | 0.011       | 0.008  | 0.046             | 0.241       | 0.042 | 0.013             | 0.080       | 0.017 |
| Pb                         | 1    | 0.004             | 0.008       | 0.009 | 0.030             | 0.081       | 0.106  | 0.179             | 0.243       | 0.172 | 0.097             | 0.306       | 0.132 |
| Cu                         | 1    | 0.001             | 0.002       | 0.026 | 0.007             | 0.029       | 0.021  | 0.129             | 0.427       | 0.105 | 0.039             | 0.200       | 0.052 |
| Al                         | 1    | 0.003             | 0.006       | 0.026 | 0.046             | 0.229       | 0.113  | 0.751             | 4.767       | 0.687 | 0.203             | 1.553       | 0.261 |
| Mn                         | 1    | 0.006             | 0.005       | 0.034 | 0.021             | 0.094       | 0.066  | 0.353             | 2.247       | 0.332 | 0.102             | 0.664       | 0.135 |
| Ni                         | 1    | 0.001             | 0.001       | 0.003 | 0.0007            | 0.002       | 0.003  | 0.005             | 0.022       | 0.005 | 0.002             | 0.008       | 0.004 |
| As                         | 1    | NA                | NA          | NA    | NA                | 0.006       | NA     | NA                | NA          | NA    | NA                | NA          | NA    |
| Fe                         | 2    | 0.001             | 0.0004      | NA    | 0.013             | 0.058       | 0.017  | 0.291             | 0.224       | 0.239 | 0.092             | 0.074       | 0.186 |
| Zn                         | 2    | 0.168             | 0.070       | NA    | 0.392             | 0.328       | 0.191  | 3.303             | 13.662      | 7.070 | 1.439             | 0.994       | 1.483 |
| Cd                         | 2    | 0.001             | 0.0006      | NA    | 0.004             | 0.003       | 0.002  | 0.031             | 0.104       | 0.053 | 0.014             | 0.009       | 0.014 |
| Pb                         | 2    | 0.003             | 0.002       | NA    | 0.044             | 0.028       | 0.025  | 0.089             | 0.046       | 0.045 | 0.113             | 0.044       | 0.078 |
| Cu                         | 2    | 0.002             | 0.0008      | NA    | 0.009             | 0.008       | 0.005  | 0.092             | 0.194       | 0.079 | 0.044             | 0.024       | 0.040 |
| Al                         | 2    | 0.001             | 0.0008      | NA    | 0.054             | 0.059       | 0.028  | 0.463             | 1.933       | 1.101 | 0.222             | 0.161       | 0.199 |
| Mn                         | 2    | 0.009             | 0.002       | NA    | 0.026             | 0.025       | 0.013  | 0.222             | 0.859       | 0.480 | 0.107             | 0.069       | 0.106 |
| Ni                         | 2    | 0.001             | 0.0004      | NA    | 0.001             | 0.0005      | 0.0002 | 0.003             | 0.008       | 0.004 | 0.002             | 0.0009      | 0.002 |
| As                         | 2    | NA                | NA          | NA    | NA                | NA          | NA     | NA                | NA          | NA    | NA                | NA          | NA    |

#### Section S4. Supplementary Information on C-Q relationships

**C-Q slopes across two years.** The slope values from C-Q relationships were compared among sites 1, 2, 3A, and 3B (**Supplementary Table S3**). These slopes provide insight into solute mobilization behavior, ranging from dilution ( $b < 0$ ), to enrichment ( $b > 0$ ), to chemostatic ( $b \approx 0$ ). Site 1 showed a wide variability across constituents, with several metals exhibiting near-zero or weakly positive slopes, indicating mixed chemostatic and enrichment behavior. This reflects its nearer to the surface position and lower storage capacity. In contrast, sites 2, 3A, and 3B displayed predominately dilution behavior across the entire sampling period, particularly for Zn, Al, and Mn. The strongest dilution slopes occurred at site 3A (e.g., Zn,  $b = -1.785$ ; Al,  $b = -1.662$ ; Mn,  $b = -1.627$ ) and site 3B (e.g., Zn,  $b = -1.580$ ; Al,  $b = -1.820$ ; Mn,  $b = -1.555$ ). The strong negative slopes indicate source-limited mobilization, suggesting solute concentrations decline rapidly with increasing discharge due to flushing of stored contaminants. DOC, pH, and EC also followed consistent dilution trends at sites 2, 3A, and 3B, reinforcing the interpretation that increased flows reduce solute concentrations via dilution and mixing with low-concentration water. Together, these C-Q slope patterns reveal spatial and temporal differences in solute sourcing that align with transient flow path activation and fill-and-spill dynamics observed in the hysteresis analysis.



**Supplementary Table S3.** Total number of constituent samples and concentration-discharge regression slopes ( $\pm$ SE) for four monitored flow sites for declining, low flow, and flush phases. NA refers to concentration values below the detection limit. All C-Q slopes are in  $\log_{10}$ - $\log_{10}$  space except for  $\delta^2\text{H}$  and  $\delta^{18}\text{O}$  which only Q is in  $\log_{10}$  space.

|                                | Site 1            |                       | Site 2            |                       | Site 3A           |                       | Site 3B           |                       |
|--------------------------------|-------------------|-----------------------|-------------------|-----------------------|-------------------|-----------------------|-------------------|-----------------------|
| Parameter                      | Total samples (n) | C-Q slope ( $\beta$ ) | Total samples (n) | C-Q slope ( $\beta$ ) | Total samples (n) | C-Q slope ( $\beta$ ) | Total samples (n) | C-Q slope ( $\beta$ ) |
| Fe (mg/L)                      | 23                | -0.160 ( $\pm$ 0.32)  | 28                | -0.994 ( $\pm$ 0.13)  | 33                | -0.140 ( $\pm$ 0.20)  | 33                | -1.443 ( $\pm$ 0.20)  |
| Zn (mg/L)                      | 25                | -0.111 ( $\pm$ 0.04)  | 28                | -0.546 ( $\pm$ 0.04)  | 33                | -1.785 ( $\pm$ 0.32)  | 33                | -1.580 ( $\pm$ 0.13)  |
| Cd (mg/L)                      | 25                | -0.187 ( $\pm$ 0.08)  | 28                | -0.550 ( $\pm$ 0.05)  | 33                | -1.522 ( $\pm$ 0.30)  | 33                | -1.533 ( $\pm$ 0.13)  |
| Pb (mg/L)                      | 25                | -0.575 ( $\pm$ 0.12)  | 28                | -0.286 ( $\pm$ 0.04)  | 33                | 0.687 ( $\pm$ 0.15)   | 33                | -0.932 ( $\pm$ 0.09)  |
| Cu (mg/L)                      | 25                | -0.070 ( $\pm$ 0.15)  | 28                | -0.555 ( $\pm$ 0.05)  | 33                | -1.156 ( $\pm$ 0.23)  | 33                | -1.367 ( $\pm$ 0.11)  |
| Al (mg/L)                      | 25                | 0.113 ( $\pm$ 0.28)   | 28                | -0.672 ( $\pm$ 0.06)  | 33                | -1.662 ( $\pm$ 0.32)  | 33                | -1.820 ( $\pm$ 0.15)  |
| Mn (mg/L)                      | 25                | 0.493 ( $\pm$ 0.09)   | 28                | -0.584 ( $\pm$ 0.05)  | 33                | -1.627 ( $\pm$ 0.32)  | 33                | -1.555 ( $\pm$ 0.13)  |
| Ni (mg/L)                      | 25                | 0.082 ( $\pm$ 0.04)   | 28                | -0.249 ( $\pm$ 0.03)  | 33                | -1.238 ( $\pm$ 0.25)  | 33                | -0.875 ( $\pm$ 0.08)  |
| As (mg/L)                      | 25                | NA                    | 28                | -0.084 ( $\pm$ 0.03)  | 33                | NA                    | 33                | NA                    |
| DOC (mg/L)                     | 25                | 0.055 ( $\pm$ 0.06)   | 28                | -0.109 ( $\pm$ 0.04)  | 33                | -0.789 ( $\pm$ 0.22)  | 33                | -0.398 ( $\pm$ 0.12)  |
| DIC (mg/L)                     | 25                | 0.097 ( $\pm$ 0.08)   | 27                | 0.023 ( $\pm$ 0.06)   | 32                | 0.201 ( $\pm$ 0.20)   | 32                | -0.100 ( $\pm$ 0.16)  |
| H <sup>+</sup> (mol/L)         | 25                | 0.701 ( $\pm$ 0.29)   | 28                | -0.460 ( $\pm$ 0.05)  | 33                | -0.360 ( $\pm$ 0.17)  | 33                | -1.027 ( $\pm$ 0.14)  |
| EC ( $\mu\text{s}/\text{cm}$ ) | 25                | 0.0172 ( $\pm$ 0.03)  | 28                | -0.239 ( $\pm$ 0.02)  | 33                | -0.687 ( $\pm$ 0.13)  | 33                | -0.682 ( $\pm$ 0.06)  |
| PLI                            | 25                | 0.0495 ( $\pm$ 0.08)  | 28                | -0.502 ( $\pm$ 0.04)  | 33                | -0.960 ( $\pm$ 0.20)  | 33                | -1.234 ( $\pm$ 0.10)  |

**Hysteresis index values for each flow phase across two years.** To capture event-scale solute transport dynamics, hysteresis index (HI) values were calculated using Llyod et al. (2016) and Zuecco et al. (2016) methods. **Supplementary Table S4** presents HI results for Fe, Zn, Cd, and PLI during two major pollution events and average overall values at sites 2, 3A, and 3B (based on the hysteresis loops in figure 5 in the main text). Site 2 consistently exhibited near to chemostatic hysteresis for Fe, Zn, Cd, and PLI overall with average HI values ranging from -0.004 (Lloyd) to -0.003 (Zuecco), indicating delayed solute mobilization and likely source zones that are geochemically buffered or spatially disconnected during rising flows. Minimal hysteresis observed during hydrologically-defined flush phases support the interpretation of single-source connectivity under limited connectivity.

At site 3A, strong counterclockwise hysteresis was observed across both main pollution events for Zn (HI = -1.230 and -0.911 using Lloyd), pointing to persistent storage-dominated transport likely from less-accessible zones. The directionality remained consistent but varied in magnitude, suggesting phase-

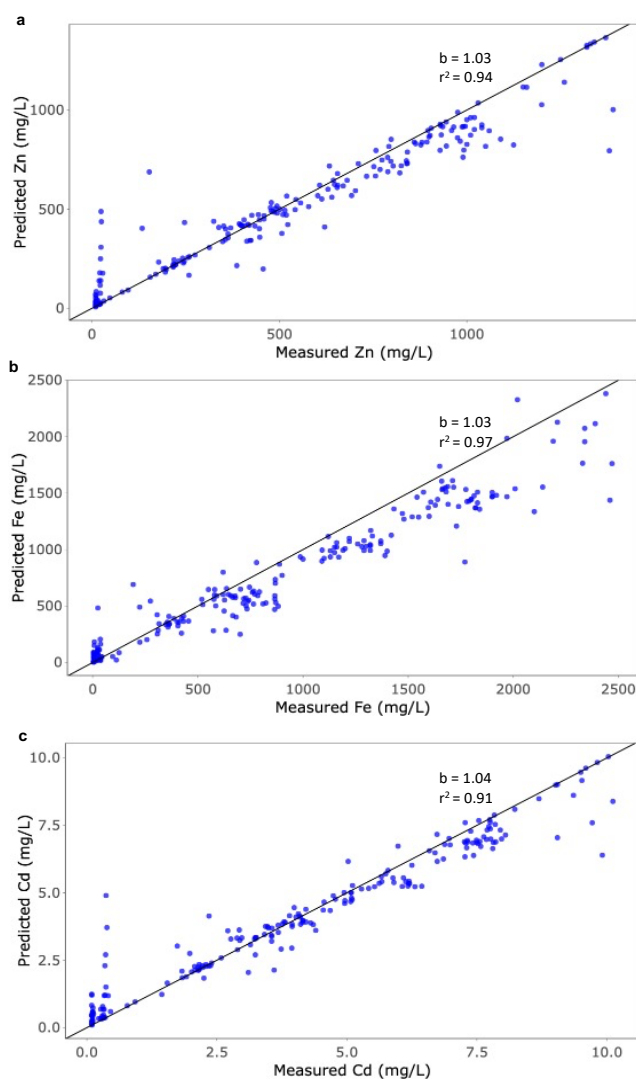
dependent release mechanisms. In contrast, site 3B showed more mixed behavior with weak to moderate counterclockwise hysteresis during both events (e.g., Cd, HI = -0.221 and -0.347). When averaged across entire monitoring periods, C-Q hysteresis patterns show minimal changes among each site, in contrast to event-based C-Q patterns. These contrasting hysteresis patterns emphasize the utility of combining HI calculation approaches and highlight how solute transport timing and source proximity evolve with hydrological conditions in legacy mine systems.

**Supplementary Table S4.** Hysteresis index values using Llyod et al. (2016) and Zuecco et al. (2016) method (abbreviated as LI and Zu) for each main pollution point and the total average (for all time points) for Fe, Zn, Cd, and PLI at sites 2, 3A, and 3B. Main pollution point 1 refers to hysteresis identification on 2022-12-20 and main pollution point 2 refers to hysteresis identification on 2023-12-12.

| Metal | Method | Site 2             |                    |           | Site 3A            |                    |           | Site 3B            |                    |           |
|-------|--------|--------------------|--------------------|-----------|--------------------|--------------------|-----------|--------------------|--------------------|-----------|
|       |        | Main poll. point 1 | Main poll. point 2 | Total avg | Main poll. point 1 | Main poll. point 2 | Total avg | Main poll. point 1 | Main poll. point 2 | Total avg |
| Fe    | LI     | -0.703             | -0.550             | -0.004    | -0.225             | -0.252             | 0.017     | -0.240             | -0.283             | 0.009     |
| Zn    | LI     | -0.090             | -0.309             | -0.004    | -1.230             | -0.911             | 0.016     | -0.184             | -0.340             | 0.008     |
| Cd    | LI     | -0.106             | -0.327             | -0.004    | -1.201             | -0.947             | 0.016     | -0.221             | -0.347             | 0.009     |
| PLI   | LI     | -0.252             | 0.025              | -0.004    | -1.026             | -0.620             | 0.017     | -0.320             | -0.410             | 0.011     |
| Fe    | Zu     | -0.497             | -0.389             | -0.003    | -0.160             | -0.178             | 0.012     | -0.170             | -0.200             | 0.006     |
| Zn    | Zu     | -0.064             | -0.219             | -0.003    | -0.869             | -0.644             | 0.012     | -0.130             | -0.240             | 0.006     |
| Cd    | Zu     | -0.075             | -0.231             | -0.003    | -0.849             | -0.670             | 0.012     | -0.156             | -0.246             | 0.006     |
| PLI   | Zu     | -0.178             | 0.018              | -0.003    | -0.726             | -0.876             | 0.012     | -0.227             | -0.290             | 0.007     |

## Section S5. Supplementary Information on cubist modeling results

**Cubist modeling.** The performance and interpretive power of the Cubist regression modeling approach that was applied using the spectrolyzer data and autosampler data is illustrated in **Supplementary Figure S3**. Figure S3 demonstrates strong agreement between measured and predicted concentrations of Zn, Fe, and Cd, with slope (b) and coefficient of determination ( $r^2$ ) values indicating robust model performance, particularly for identifying peak events and transitions between flow regimes.



**Supplementary Figure S3.** Measured (from the autosampler) versus predicted dissolved concentrations for (a) Zn, (b) Fe, and (c) Cd from cubist modeling results and goodness of fit line is shown. The calculated slope (b) and coefficient of determination ( $r^2$ ) values are presented.

## References

- Baumann, P. (2020): simplerspec: soil and plant spectroscopic model building and prediction, available at: <https://github.com/philipp-baumann/simplerspec>, last access: 1 May 2025.
- Craig, H.: Isotopic Variations in Meteoric Waters, Reinhold, 1934.
- Henderson, F. M.: Open Channel Flow, MacMillan, New York, 1966.
- Kuhn, M.: Building predictive models in R using the caret package, Journal of Statistical Software, 28, 1–26, <https://doi.org/10.18637/jss.v028.i05>, 2008.
- Kuhn, M. and Quinlan, R. (2023): Cubist: rule- and instance-based regression modeling, available at: <https://CRAN.R-project.org/package=Cubist>, last access: 1 May 2025.
- Lloyd, C. E. M., Freer, J. E., Johnes, P. J., and Collins, A. L.: Technical Note: Testing an improved index for analysing storm discharge–concentration hysteresis, Hydrol. Earth Syst. Sci., 20, 625–632, <https://doi.org/10.5194/hess-20-625-2016>, 2016.
- Spangenberg, J. E., Dold, B., Vogt, M. L., and Pfeifer, H. R.: Stable hydrogen and oxygen isotope composition of waters from mine tailings in different climatic environments, Environmental Science and Technology, 41, 1870–1876, <https://doi.org/10.1021/es061654w>, 2007.
- Stevens, A. and Ramirez-Lopez, L. (2022): An introduction to the prospectr package, available at: <https://cran.r-project.org/web/packages/prospectr/index.html>, last access: 1 May 2025.
- Swenson, L. J., Zipper, S., Peterson, D. M., Jones, C. N., Burgin, A. J., Seybold, E., Kirk, M. F., and Hatley, C.: Changes in Water Age During Dry-Down of a Non-Perennial Stream, Water Resources Research, 60, <https://doi.org/10.1029/2023wr034623>, 2024.
- Zuecco, G., Penna, D., Borga, M., and Meerveld, H. J. van: A versatile index to characterize hysteresis between hydrological variables at the runoff event timescale, Hydrol. Process., 30, 1449–1466, <https://doi.org/10.1002/hyp.10681>, 2016.